ACS NANO

www.acsnano.org

ARTICLE

Probing Interlayer Interactions and Commensurate–Incommensurate Transition in Twisted Bilayer Graphene through Raman Spectroscopy

Vineet Pandey, Subhendu Mishra, Nikhilesh Maity, Sourav Paul, Abhijith M. B, Ajit K. Roy, Nicholas R. Glavin, Kenji Watanabe, Takashi Taniguchi, Abhishek K. Singh,* and Vidya Kochat*

Cite This: *ACS Nano* 2024, 18, 4756–4764

Read Online

ACCESS | Metrics & More | Article Recommendations | Supporting Information

ABSTRACT: Twisted 2D layered materials have garnered much attention recently as a class of 2D materials whose interlayer interactions and electronic properties are dictated by the relative rotation/twist angle between the adjacent layers. In this work, we explore a prototype of such a twisted 2D system, artificially stacked twisted bilayer graphene (TBLG), where we probe, using Raman spectroscopy, the changes in the interlayer interactions and electron–phonon scattering pathways as the twist angle is varied from 0° to 30°. The long-range Moiré potential of the superlattice gives rise to additional intravalley and intervalley scattering of the electrons in TBLG, which has been investigated through their Raman signatures. Density functional theory (DFT) calculations of the electronic band structure of the TBLG superlattices were found to be in agreement with the resonant Raman excitations across the van Hove singularities in the valence and conduction bands predicted for TBLG due to hybridization of bands from the two layers. We also observe that the relative rotation between the graphene layers has a marked influence on the second order overtone and combination Raman modes signaling a commensurate–incommensurate transition in TBLG as the twist angle increases. This serves as a convenient and rapid characterization tool to determine the degree of commensurability in TBLG systems.

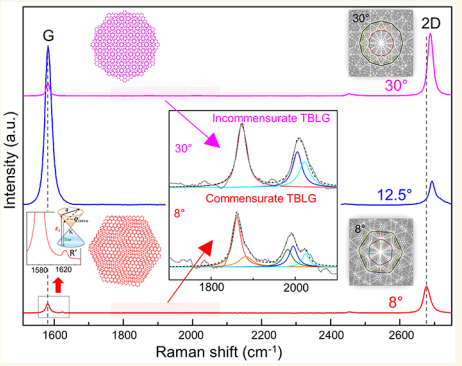

KEYWORDS: *twisted bilayer graphene, Raman spectroscopy, combination modes, density functional theory, commensurate–incommensurate transition*

Two-dimensional layered materials with twist dependent stacking have been a hot topic of research recently, as the electronic properties of such systems critically depend on the superlattice formation due to relative rotation between the layers. A prototype system, twisted bilayer graphene (TBLG) has been a typical example of the superlattice-induced modified band structure exhibiting emergent phases such as correlated insulator, superconductivity, and ferromagnetism emerging at critical twist angles called the magic angles.[1−4] In a TBLG Moiré superlattice, alternating AA and AB stacked regions emerge, leading to a hexagonal superlattice potential that folds the bands into a mini-Brillouin zone. The adjacent Dirac cones in this mini-Brillouin zone hybridize leading to bands with reduced Fermi velocity near charge neutrality point, furthermore developing into flat bands for critical angles close to 1.1° or the magic angles.[5] For small values of twist angles, the atoms adjust with the superlattice landscape forming an energetically favorable commensurate system, by gaining van der Waals energy, but at the expense of elastic energy. As the Moiré period becomes smaller, the van der Waals energy gain over the elastic energy loss is no longer compensated, leading to an incommensurate system of bilayers, where each layer is independent of the other.[6] This shows that the mechanical and electronic degrees of freedom are closely related in TBLG systems, wherein the twist angle determines the modifications to the band structure and also the interlayer coupling.

Received: September 2, 2023
Revised: January 24, 2024
Accepted: January 25, 2024
Published: January 31, 2024

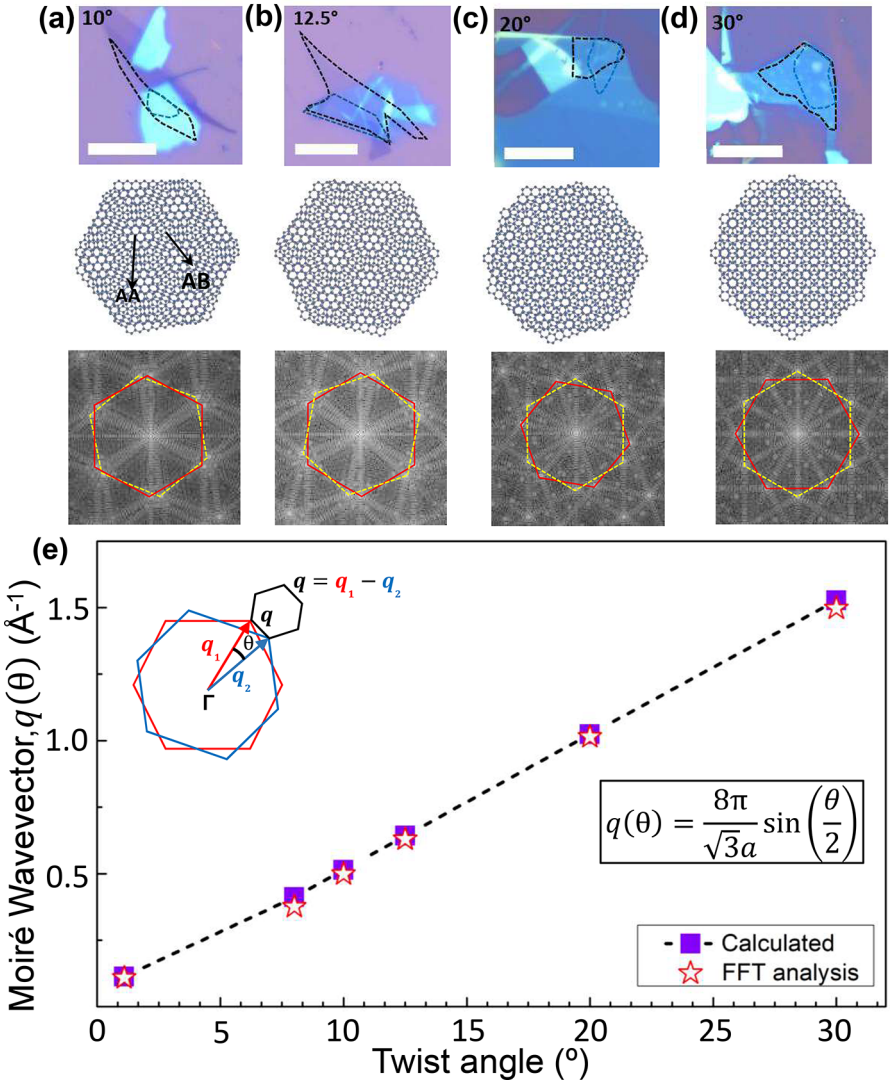

Figure 1. (a–d) Optical images of samples (first row; scale: 10 μm), real space lattice structures (second row), and FFT analysis with reciprocal space representing first Brillouin zone separation (third row) for 10°, 12.5°, 20°, and 30° TBLG samples. (e) Plot of $q(\theta)$ vs θ for twist angles ranging from 1.1° to 30° TBLG samples showing the values calculated by the formula in the inset and obtained from the FFT analysis of Moiré wavevector $q(\theta)$ as shown in the inset figure.

The 2D quantum materials-based technology projections are focused on identifying artificially stacked 2D heterostructures with combined and novel functionalities of various 2D materials. In this context, it becomes very important to understand how the twist degree of freedom between the layers determines the fundamental properties such as mechanical coupling, elasticity, electronic band structure, and electron–phonon coupling in such 2D heterostructure stacks. In this work, we have investigated these properties in twisted graphene bilayers, which is a very promising system of homobilayers exhibiting rich variation of the electronic properties with changing relative rotation between the layers. While at low angles emergent phases attributed to flat bands have been observed, at high angles close to 30° TBLG forms an incommensurate superlattice with quasi-crystalline order and mirrored Dirac cones originating from strong interlayer interaction.[7−9] Significant experimental effort has gone into studies of the Moiré superlattices in TBLG concentrating on STM and ARPES.[10−20] We have studied the effect of the Moiré potential on the interlayer coupling and band structure by using Raman spectroscopy, which is a well-established powerful characterization technique to investigate the layer numbers, disorder, and stacking orientations in bi- and trilayer graphene systems.[21−26] Raman studies on folded graphene and chemical vapor deposition (CVD) grown rotationally stacked bilayer graphene showed emergence of additional modes due to the intravalley and intervalley scattering of electrons by Moiré potential.[27−37] Also it was found that Raman studies as a function of laser energy and twist angle can trace the positions of the van Hove singularities (vHs) in the conduction and valence bands of TBLG originating from the hybridization of the Dirac cones of the twisted graphene layers.[38−40] Modifications of the electronic band structure and the phonon dispersion in TBLG was suggested to give rise to frequency shifts of the 2D peak as well as the line shape and width.[41−46] On the other hand, the Raman studies in artificially stacked bilayer graphene systems have been very limited. Similar observations were noted in twisted CVD bilayers fabricated by PMMA-assisted transfer, while in artificially stacked exfoliated bilayer graphene, studies reported variations of in-plane

https://doi.org/10.1021/acsnano.3c08344
ACS Nano 2024, 18, 4756−4764

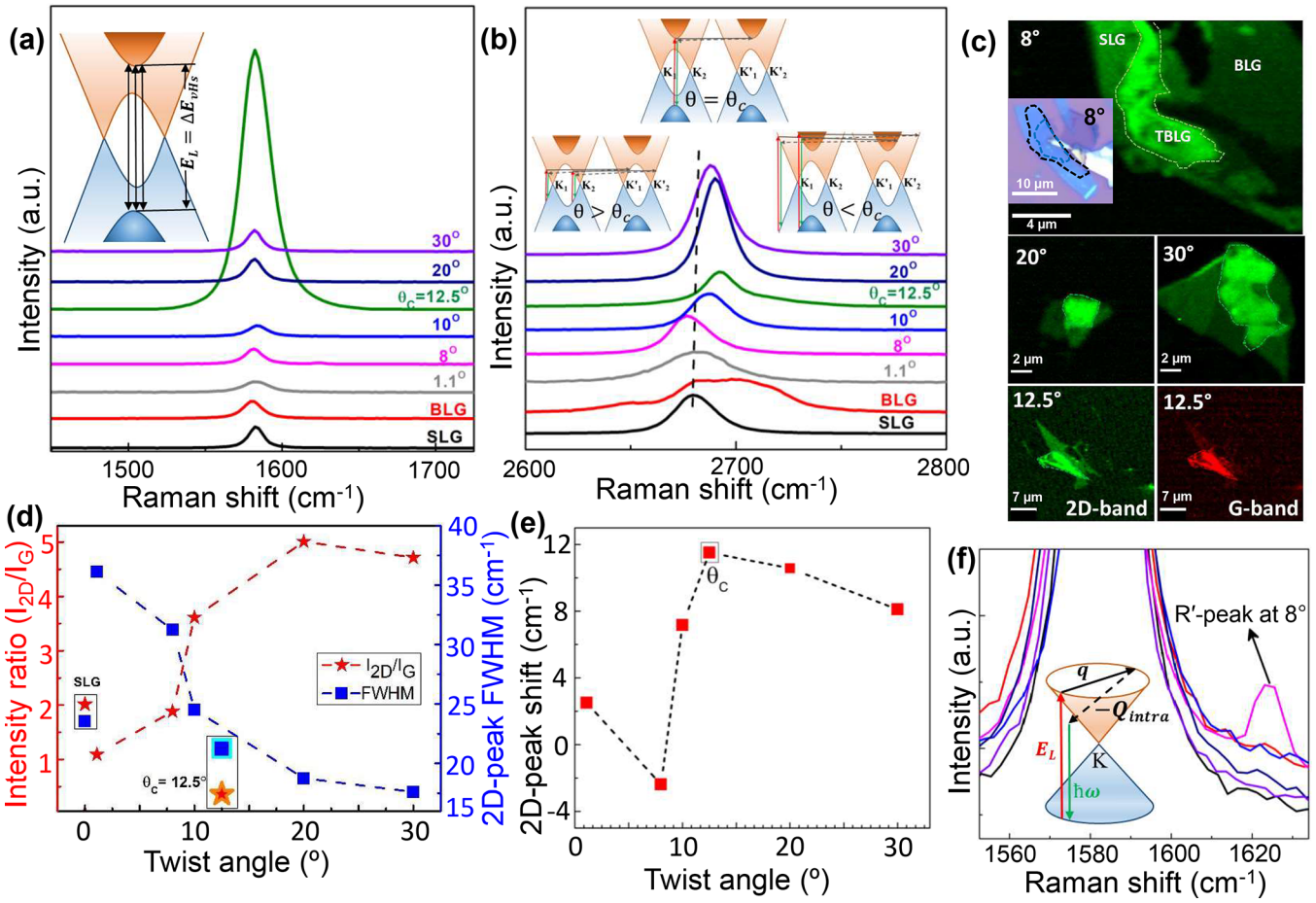

Figure 2. (a) Raman shift of G-peak for all TBLG samples. G-peak enhancement occurs for $\theta_C = 12.5°$ due to parallel band transitions (inset figure) at $E_L = \Delta E_{vHs}$. (b) Raman shift of the 2D peak for all TBLG samples. The various intervalley scattering possibilities occurring for $\theta > \theta_C$, $\theta = \theta_C$, and $\theta < \theta_C$ are shown in the inset. (c) Raman maps of the 2D peak (green) for different TBLG samples. Raman map for the G peak (red) shows a resonance enhancement for 12.5° TBLG. (d) Plot for I_{2D}/I_G and 2D-peak fwhm as a function of twist angle θ is shown for different TBLG samples. (e) Plot of 2D-peak shift of TBLG relative to the SLG as a function of twist angle, θ. (f) Appearance of R′-peak for 8° TBLG sample along with the intravalley scattering process due to Moiré potential as depicted in the inset.

anisotropy and superlattice-induced transverse acoustic Raman modes with the misorientation angle.[47,48] For TBLG close to magic angles, the G and 2D bands were significantly influenced by the electron−phonon interactions and the areal coverage of AB and BA stacked regions separated by strain soliton regions.[49]

In this work, we have studied the electron−phonon scattering mechanisms in artificially stacked TBLG in detail and substantiated our results with those of folded and CVD grown graphene Raman signatures. The various intravalley and intervalley scattering mechanisms induced by Moiré potential have been investigated, and the results have been explained by variations in the electronic band structure and density of states (DOS) obtained from density functional theory (DFT) calculations. In addition, we observe that the resonance arising from the transition between the vHs in the valence and conduction band also presents interesting features in G and M bands. Our work shows that the tunability of the vHs in rotationally misoriented bilayer graphene can give rise to enhanced absorption leading to wavelength selective photodetectors in the future. Finally we also explore the overtone and combination modes in TBLG which serve as a definitive signature of commensurate to incommensurate transition at higher twist angles and mechanical decoupling of the layers.

RESULTS AND DISCUSSION

The TBLG samples were fabricated using the tear and stack method using a 2D transfer system (from CryoNano Laboratories) for various twist angles as shown in the optical micrographs in the top panels of Figure 1a−d.[50] The middle panel shows the superlattice evolution for the corresponding angles from which it is evident that at low angles (<12.5°) a long-range Moiré pattern evolves and the TBLG can be approximately treated as a system with Moiré period governed translational symmetry. At larger twist angles (>20°), the Moiré period is on the order of atomic length scale evolving to a quasi-crystalline (QC) state at twist angles of 30°. The FFT of these TBLG systems gives a direct estimation of the Moiré wavevector, **q**, whose magnitude is plotted in Figure 1e. The QC TBLG lattice, which lacks translational symmetry, shows a 12-fold rotational order in the FFT analysis. A geometrical analysis in the reciprocal space reveals that the additional periodicity due to the Moiré potential results in a mini-Brillouin zone with a twist angle (θ) dependent lattice vector which is the result of the wavevectors $\mathbf{q}_1$ and $\mathbf{q}_2$ corresponding to the top and bottom layers and is given by

$$q(\theta) = \frac{8\pi}{\sqrt{3}\,a} \sin\left(\frac{\theta}{2}\right) \quad (1)$$

https://doi.org/10.1021/acsnano.3c08344
ACS Nano 2024, 18, 4756−4764

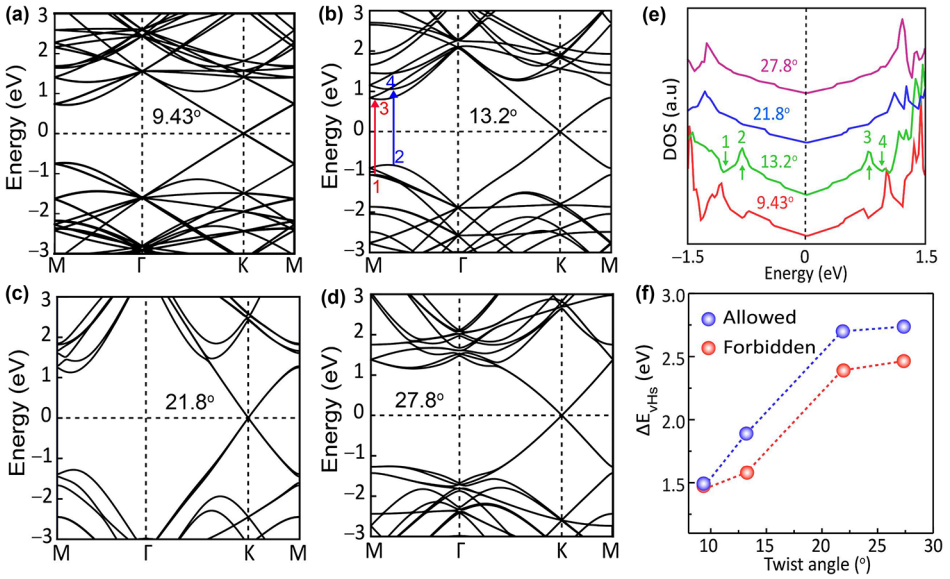

Figure 3. Electronic band structure of TBLG for twist angles of (a) 9.43°, (b) 13.2°, (c) 21.8°, and (d) 27.8°, respectively. The red and blue arrows in panel b represent the allowed (1 → 3 or 2 → 4) optical transitions. (e) Calculated total DOS of TBLG for twist angles 9.43°, 13.2°, 21.8°, and 27.8°. The allowed (1 → 3 or 2 → 4) is given for 13.2°. (f) Value of ΔE_{vHs} of allowed (1 → 3 or 2 → 4) and lowest forbidden transitions (2 → 3) in TBLG for twist angles 9.43°, 13.2°, 21.8°, and 27.8° respectively.

where a = 0.246 nm is the lattice parameter of graphene.[29] The values obtained for $q(\theta)$ from this calculation perfectly match the values obtained directly from the FFT analysis as can be seen from Figure 1e.

The TBLG samples were studied through Raman spectroscopy using 532 nm excitation, and the spectra corresponding to the twist angles 1.1°, 8°, 10°, 12.5°, 20°, and 30° are shown in Figure 2a,b along with a single layer graphene (SLG) and Bernal-stacked bilayer graphene (BLG). The G peak arising from the doubly degenerate zone center E_{2g} mode occurs at 1582 cm^{-1} and shows a negligible frequency shift with the twist angle. Interestingly at twist angle of 12.5°, we observe a huge enhancement of the G-peak intensity. Such an enhancement has been reported earlier in CVD grown bilayer graphene samples at misorientation angles of 10° to 12° under 633 and 532 nm excitation.[30,40,42] This has been attributed to the resonant condition when the laser excitation energy matches the parallel band singularity in TBLG. Here there are a large number of states with the same energy difference, giving rise to Raman scattering paths with identical phases that interfere constructively and result in considerable enhancement of the G peak.[39,46] When the Dirac cones of the top and bottom layers overlap, the DOS is modified due to the interactions leading to hybridization gap, and vHs emerge in the conduction and valence bands of TBLG. When the excitation laser energy E_L matches this energy separation between the conduction and valence band vHs, which in turn is dependent on the twist angle θ, resonance occurs as per the condition

$$\theta_C = \frac{3aE_L}{\hbar v_f 4\pi} \quad (2)$$

where v_f is the Fermi velocity in SLG (10^6 m/s) and θ_C is the critical twist angle. For an excitation wavelength of 532 nm (2.33 eV), $\theta_C \sim 12.3°$, which matches well with the twist angle where the resonance is observed experimentally. This is also the first observation of G-peak resonance in TBLG fabricated by the tear and stack method. In the Raman map in Figure 2c (given in red, bottom panel), the G-peak resonance is clearly observable in the TBLG region, whereas the region of the SLG has much lower intensity. We show later that this picture of parallel bands is in accordance with the band structure obtained from DFT simulations as well.

As opposed to the G peak, the 2D peak shows significant variations in frequency and intensity as a function of the twist angle. An interesting aspect of the 2D peak is the single Lorentzian behavior in TBLG which is in contrast with the convoluted peak picture for the Bernal-stacked BLG.[21,49] It proves that the Dirac nature of the bands from individual layers is retained at higher twist angles. With increase in twist angle, the intensity ratio of the 2D peak to the G peak, I_{2D}/I_G increases to about 4 times that of SLG, while the fwhm of the single Lorentzian reduces and becomes similar to that of SLG as shown in Figure 2d. At low twist angle of 1.1°, we observe a broad single 2D peak which is blue-shifted in comparison to the 2D peak of SLG. Previous studies have attributed this blue shift to reduction in Fermi velocity in TBLG for twist angles below <5°.[40,41,51−53] With an increase in twist angle, this blue shift initially reduces but again increases at twist angles larger than 10°. The maximum blue shift occurs at θ_C and decreases at lower and higher twist angles as seen in the plot in Figure 2e. The variations in the intensity, fwhm, and shifts of the 2D peak can be attributed to the differences in the scattering mechanisms as a function of twist angle described in the schematics in Figure 2b. For $\theta > \theta_C$, the separation between the vHs, $\Delta E_{vHs} > E_L$ and hence the energy dispersion is linear with negligible interaction between the layers. The iTO phonons contribute to the double resonance process of intralayer intervalley scattering between the K and K′ valleys of the two layers. Since the frequencies of the scattering phonons, energy dispersion, and electron−phonon coupling are all identical for the two layers, the resulting 2D peak should have a higher intensity than SLG and also similar fwhm. At $\theta = \theta_C$, $\Delta E_{vHs} \approx E_L$, and a large number of optical transitions occur due to the vHs, which increases the joint DOS. There is also a transition from linear dispersion to a flat band dispersion, due

https://doi.org/10.1021/acsnano.3c08344
ACS Nano 2024, 18, 4756−4764

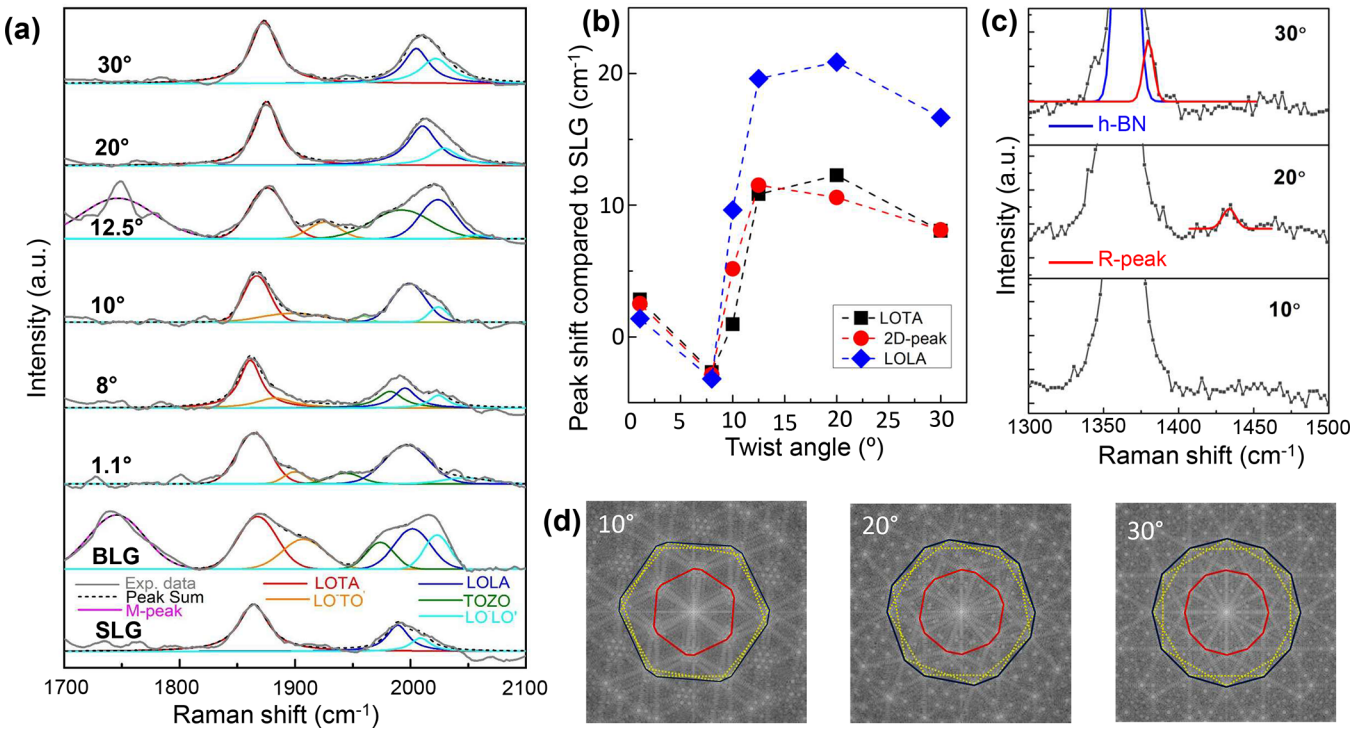

Figure 4. (a) Plot of Raman shift for M band and combination modes (near 1860 and 2000 cm^{-1}) in different TBLG samples. Peak-fitting of the data identifies all the possible combination modes. (b) Raman peak shift of TBLG compared to SLG for LOTA, LOLA, and 2D peaks for different TBLG samples. (c) R peak (in red) appears for 20° and 30° at 1435 and 1375 cm^{-1} respectively. (d) In the Fourier space, the transition of the TBLG system from commensurate lattice (10°) to incommensurate lattice (20° and 30°) is shown. The rotational symmetry is near 6-fold for 10° gradually reaching 12-fold for 30°, which is also a quasi-crystalline state.

to which the phonons giving rise to intervalley scattering have larger wavevectors which also explains the huge blue shift of the 2D peak at θ_C. The flat band and the joint DOS also give rise to slight variations in the wavevectors of the scattering phonons leading to an increased fwhm. Finally, at $\theta < \theta_C$, $\Delta E_{vHs} < E_L$ due to the increased interlayer interactions, along with intralayer scattering, interlayer intervalley scattering is also possible. This gives rise to a complex interference between the scattered phonons, reducing the intensity and increasing the fwhm at low twist angles as observed in Figure 2d. The 2D Raman maps for the various twist angles are shown in Figure 2c, which clearly indicate that the intensity is uniform throughout the entire TBLG region and also are good experimental proof for a spatially homogeneous superlattice structure.

At low angles of 8°, we observe an additional peak at 1625 cm^{-1}, which is absent for higher twist angles as shown in Figure 2f. This peak is attributed to the R′-peak which arises due to the intravalley double resonance process, where the excited electron is elastically scattered by its interaction with the Moiré potential through the rotational wavevector, $q(\theta)$, to the point in the same valley with equal and opposite momentum. A phonon with a wavevector the same as $q(\theta)$ given by Q_{intra} is created and scatters the electron back inelastically, which finally combines with a hole to give the Raman shift observed. From the phonon dispersion curve of graphene, we observe that Q_{intra} corresponds to the LO phonon frequency of 1625 cm^{-1} which lies close to the Γ point in the first Brillouin zone along the ΓK direction and has strong electron−phonon coupling.[29,54] For this type of intravalley scattering for a twist angle of θ, the incident photon energy is given by

$$E_L^{intra}(\theta) = \hbar v_F q(\theta) \quad (3)$$

For E_L^{intra} = 2.33 eV, $q(\theta)$ turns out to be 0.365 $Å^{-1}$ corresponding to a twist angle of 7.1° from Figure 1e, which is very close to the experimental twist angle of 8°.

The experimental Raman signatures have also been corroborated by first-principles DFT calculations performed using the Vienna ab initio simulation package (VASP).[55,56] The electronic band structure of SLG has a linear band dispersion in the vicinity of high-symmetry point K and results in 4-fold degenerate states from the p_z orbital of the carbon atom. On the other hand, in TBLG, at energies far from the Fermi level, the bands are modified and split, resulting in the appearance of extrema for some of the sub-bands close to the M point in the Brillouin zone as indicated by 1, 2, 3, and 4 in Figure 3b.[57] These saddle points near the M point in the band structure of TBLG result in twist-induced spikes (singularity 2 and 3) and twist-induced kinks (singularity 1 and 4) in the DOS known as vHs shown in Figure 3e. These saddle points/vHs play an important role in determining the optical transitions when light is incident on these systems. These vHs differences (ΔE_{vHs}) give information on the strength and the energy of the transitions. In TBLG, the allowed transitions are from 1 to 3 and 2 to 4, while 1 to 4 and 2 to 3 transitions are forbidden.[58] The ΔE_{vHs} variation with twist angle of TBLG for allowed and forbidden transitions is given in Figure 3f. From Figure 3f, it is observed that the vHs splitting increases with increasing twist angle of TBLG, which is consistent with the previous literature.[59] When the excitation laser energy E_L matches the energy separation between the conduction and valence band vHs of the allowed transition (transitions 1 → 3 or 2 → 4), a large number of excitations occur. The calculated

https://doi.org/10.1021/acsnano.3c08344
ACS Nano 2024, 18, 4756−4764

allowed transition energies of TBLG for twist angles 9.43°, 13.2°, 21.8°, and 27.8° are 1.46, 1.89, 2.70, and 2.74 eV, respectively. The experimental E_L is very close to the calculated ΔE_{vHs} corresponding to TBLG with a twist angle 13.2°. Therefore, our theoretical observation suggests that the closest resonance ($E_L \approx \Delta E_{vHs}$) for laser energy of 2.33 eV occurs in the vicinity of θ = 13.2°, consistent with our experimental result and θ_C = 12.3° calculated based on the continuum model.[36] Hence, our theoretical study and experimental observation indicate that the resonance of E_L with ΔE_{vHs} is the fundamental reason for the enhancement of the G peak in TBLG at a twist angle of 12.5°.

Apart from the first order Raman modes, we also investigated the second order peaks and combination modes, which also yield crucial information regarding the layer stacking. Specifically, we have looked into the Raman spectrum in the range of 1700 cm^{-1} to 2100 cm^{-1} in TBLG and compared it with those of SLG and Bernal-stacked BLG as shown in Figure 4a. In BLG, a peak is observed at 1750 cm^{-1} which is the M band, an overtone of the oTO phonon giving rise to an electron double resonant intravalley scattering. This mode becomes Raman active due to interlayer coupling. Hence it is absent in SLG, but present in BLG, multilayer graphene, and graphite with Bernal stacking.[60] We find that the M band is absent in TBLG samples, clearly indicating deviations from Bernal stacking, which renders the oTO phonon Raman inactive. The absence of the M band indicates significant weakening of the interlayer interactions as compared to Bernal-stacked BLG. Surprisingly, we observe the M band for a twist angle of 12.5°. It has been shown that the M band can selectively be seen in single-walled carbon nanotubes (SWCNTs) of certain chiralities and diameters when the laser excitation energy matches the transition energy between the valence and conduction band vHs.[61,62] On a similar vein, the observation of the M band coinciding with the G-peak resonance enhancement suggests its origin related to the resonant excitation between vHs and inelastic scattering involving oTO phonons. From the schematics in Figure 2b, we can see that for $\theta < \theta_C$ and $\theta > \theta_C$, the excitation occurs between the linear energy regimes of the two Dirac cones of the graphene layers comprising the TBLG. In this regime there is no hybridization of the Dirac cones of the two graphene layers and hence essentially this can be treated as two isolated graphene layers where the oTO phonon is inactive. At $\theta = \theta_C$, the resonant excitation occurs between the vHs emerging out of the strong hybridization or coupling of the Dirac cones of the graphene layers, which can render the M band active.

We also investigated the reported combination modes around 1860 and 2000 cm^{-1} for the TBLG samples.[63,64] These modes are shown for TBLG samples along with SLG and BLG in Figure 4a. The nomenclature of the various phonons giving rise to these combination modes is given in Table 1. At 1860 cm^{-1}, we observe that for the BLG, there are two convoluted peaks corresponding to LO^-TA (LOTA@Γ) and LO^-TO'@Γ which reduces to a single narrow peak attributed to LOTA@Γ in SLG. As the twist angle increases, we observe the reduction in intensity of the peak corresponding to LO^-TO'@Γ. In BLG, around 2000 cm^{-1}, the phonon contributions around the Γ and K points are comparable leading to a band which is a convolution of three peaks corresponding to scattering by the phonon modes LO^+LA@Γ, LO^-LO'@Γ, and TOZO@K. The peak corresponding to TOZO@K vanishes for the SLG as a result of

Table 1. Combination Modes between 1860 and 2000 cm^{-1} for the TBLG Samples

combination modes	vibrational Raman modes	significance
iLO + iTO or iLO^+ + iTO^+	E_g	doubly degenerate in-plane symmetric with in-phase and out-of-phase displacement
ZO′ and ZO^+	A_{1g}	nondegenerate out-of-plane symmetric with in-phase and out-of-phase displacement
ZA and ZO^-	A_{2u}	nondegenerate out-of-plane antisymmetric with in-phase and out-of-phase displacement
LA + TA and LO^- + TO^-	E_u	doubly degenerate in-plane antisymmetric with in-phase and out-of-phase displacement

negligible electron−phonon coupling of ZO^-@K, while the interlayer interactions restore this mode in BLG.[60] At high twist angles, we observe the absence of the Raman peak from TOZO@K. Altogether, we find that above 12.5° twist angle, the Raman modes in the range of 1700 cm^{-1} to 2100 cm^{-1} resemble those of SLG. This suggests the transition from a commensurate (C-TBLG) to an incommensurate (I-TBLG) sublattice with increasing rotational misorientation. We also observe a significant blue shift of the phonon modes associated with LOTA and LOLA at higher twist angles when compared to that of SLG as shown in Figure 4b. This shows a stiffening of the phonon modes possibly due to a compressive strain in I-TBLG as opposed to the C-TBLG. The blue shift of the combination modes also follows the same variation as that of 2D peak. In addition to Fermi velocity renormalization (at low twist angles <5°) and variations in band curvature (around θ_C = 12°), the compressive strain arising from incommensurability at large twist angles is another reason for the observed blue shift in the 2D peak and the combination modes. Such blue shift of the 2D peak has also been observed earlier in h-BN encapsulated graphene with incommensurate superlattice structure.[65] 30° TBLG is considered to be a quasicrystal with no long-range translational symmetry but rotational symmetry being preserved with a dodecagonal pattern of arrangement that can also be inferred from the reciprocal space as shown in Figure 4d. The evolution from the 6-fold symmetry at 10° to the 12-fold symmetry at 30° is represented in the reciprocal space in Figure 4d. From the combination mode Raman spectrum and symmetry analysis of the reciprocal space, we conclude that TBLG with a twist angle of 20° behaves as an incommensurate lattice with no quasicrystalline symmetry.

Even though the interlayer interactions are weakened in the I-TBLG, it is important to see if there is any contribution of the Moiré potential to the electron scattering mechanisms in the two layers. To study this, we have looked for signatures of predicted R-peak arising from the intervalley double resonant scattering. Here an excited electron is elastically scattered to another inequivalent valley by a large rotation momentum $q(\theta)$ and then inelastically backscattered to the same k value by a zone boundary phonon Q_{inter}, followed by recombination with a hole giving the Raman scattered photon.[29] Near the K point, the TO phonon branch has very strong electron−phonon coupling and provides the momentum required for the intervalley scattering. For twist angles of 30° and 20°, we observe low intensity peaks at ∼1375 cm^{-1} and ∼1435 cm^{-1}, respectively, in the Raman spectrum shown in Figure 4c which also matches with the predicted values for the R peaks. This

https://doi.org/10.1021/acsnano.3c08344
ACS Nano 2024, 18, 4756−4764

shows that even in incommensurate lattices the Moiré potential can influence the electron scattering mechanisms.

CONCLUSIONS

In conclusion, we have carried out detailed Raman spectroscopic investigations of TBLG and found clear Raman signatures which can be correlated with the changes in the electronic bands due to the Moiré potential induced by twisting the graphene layers. When the laser excitation matches the energy separation between the vHs arising from hybridization between the bands of the two layers, resonance features arise in the G peak and the M band in TBLG. The Moiré potential can also induce intra- and intervalley scattering processes giving rise to twist angle specific peaks in the Raman spectrum of TBLG. The observed upshift of the 2D peak and combination modes at high twist angles can be attributed to the compressive strain in incommensurate superlattice. The 2D peak intensity and fwhm, together with the Raman spectrum of the combination modes, can jointly distinguish between commensurate and incommensurate superlattices formed in TBLG making this a valuable characterization technique to investigate the degree of commensurability in graphene-based 2D heterostructures.

METHODS

Sample Preparation. The SLG and BLG used in the experiments were obtained from mechanical exfoliation of bulk graphite of graphenium grade with high purity from HQ graphene. The TBLG samples were fabricated using the tear and stack technique detailed in the Supporting Information.

Raman Measurements. Raman scattering measurements were performed using the WITEC alpha300 system equipped with an 1800 lines/mm grating. The excitation was performed using a 532 nm diode laser with a power of approximately 16.87 mW and a spot size of 500 nm. To observe the samples, a 100× objective lens with a 0.95 NA was utilized, and the intensity was detected using a CCD. The data analysis was carried out using the WITEC Project software.

DFT Calculations. In order to gain insights into the changes in the interlayer interactions and electron−phonon scattering of TBLG with twist angle, first-principles DFT calculations were performed using VASP.[55,56] The all-electron projector augmented wave (PAW) potentials were used to represent the ion−electron interactions in the TBLG systems.[66,67] For the calculations, the electronic exchange and correlation part of the potential was described by the Perdew−Burke−Ernzerhof (PBE) generalized gradient approximation (GGA).[68] A 20 Å vacuum was used along the *c*-axis in order to avoid spurious interactions between periodically repeated images of single layer and bilayer TBLG systems. The Kohn−Sham orbitals were expanded using the plane wave basis sets with an energy cutoff of value 500 eV. All structures were relaxed using the conjugate-gradient algorithm until the Hellmann−Feynman forces on every atom were less than 0.005 eV $Å^{-1}$. For bilayer graphene and TBLG, the lattice parameters and atomic positions were optimized by considering the weak van der Waals (vdW) interactions between the layers as implemented in Grimme's PBE-D2.[69] For relaxation, a well-converged Monkhorst−Pack (MP) k-grid of 12 × 12× 1 was used to sample the Brillouin zone (BZ) of SLG and BLG.[70] For TBLG of twist angles 27.8° and 21.8°, a k-grid of 8 × 8 × 1 was used, and for 13.2° and 9.43° twist angles, a 6 × 6 × 1 k-grid was used.

ASSOCIATED CONTENT

Supporting Information

The Supporting Information is available free of charge at https://pubs.acs.org/doi/10.1021/acsnano.3c08344.

Details of crystal geometry used to do DFT calculations of different TBLG systems; band structure of SLG and BLG; phonon band structure of SLG and TBLG systems using DFT; detailed fabrication method for TBLG using the tear−stack method (PDF)

AUTHOR INFORMATION

Corresponding Authors

Abhishek K. Singh − *Materials Research Centre, Indian Institute of Science, Bengaluru 560012, India;* orcid.org/0000-0002-7631-6744; Email: abhishek@iisc.ac.in

Vidya Kochat − *Materials Science Centre, Indian Institute of Technology, Kharagpur, West Bengal 721302, India;* orcid.org/0000-0002-6144-3732; Email: vidya@matsc.iitkgp.ac.in

Authors

Vineet Pandey − *Materials Science Centre, Indian Institute of Technology, Kharagpur, West Bengal 721302, India*

Subhendu Mishra − *Materials Research Centre, Indian Institute of Science, Bengaluru 560012, India*

Nikhilesh Maity − *Materials Research Centre, Indian Institute of Science, Bengaluru 560012, India*

Sourav Paul − *Materials Science Centre, Indian Institute of Technology, Kharagpur, West Bengal 721302, India*

Abhijith M. B − *Materials Science Centre, Indian Institute of Technology, Kharagpur, West Bengal 721302, India*

Ajit K. Roy − *Air Force Research Laboratory, Wright-Patterson Air Force Base, Dayton, Ohio 45433, United States*

Nicholas R. Glavin − *Air Force Research Laboratory, Wright-Patterson Air Force Base, Dayton, Ohio 45433, United States;* orcid.org/0000-0002-9447-7509

Kenji Watanabe − *Research Center for Electronic and Optical Materials, National Institute for Materials Science, Tsukuba 305-0044, Japan;* orcid.org/0000-0003-3701-8119

Takashi Taniguchi − *Research Center for Materials Nanoarchitectonics, National Institute for Materials Science, Tsukuba 305-0044, Japan;* orcid.org/0000-0002-1467-3105

Complete contact information is available at: https://pubs.acs.org/10.1021/acsnano.3c08344

Notes

A preprint version of this manuscript is available: Pandey, V.; Mishra, S.; Maity, N.; Paul, S; B, A. M.; Roy, A.; Glavin, N. R.; Watanabe, K.; Taniguchi, T.; Singh, A. K.; Kochat, V. Probing interlayer interactions and commensurate-incommensurate transitionin twisted bilayer graphene through Raman spectroscopy. *arXiv* 2023, 2311.01029, arxiv:cond-mat. https://doi.org/10.48550/arXiv.2311.01029 (accessed Nov 2,2023).
The authors declare no competing financial interest.

ACKNOWLEDGMENTS

VP, SP, AMB and VK acknowledge the funding from the Startup Research Grant from Science and Engineering Research Board (SERB), Department of Science and Technology (DST), Government of India and the STEP facility, IIT Kharagpur. VK, NG and AR acknowledge funding from AOARD (Asian Office of Aerospace Research and Development) under Grant No. FA2386-21-1-4014. SM, NM, and AKS thank the Materials Research Centre (MRC), Supercomputer Education and Research Centre (SERC), and Solid State and Structural Chemistry Unit (SSCU), Indian Institute of Science, Bangalore, for providing the required

computational facilities. SM, NM, and AKS also acknowledge support from The Institute of Eminence (IoE) scheme of The Ministry of Human Resource Development (MHRD), Government of India and SERB grant (File Number: CRG/2021/000633)from DST, Government of India for financial support. VP, SP, AMB, VK, SM, NM and AKS also acknowledge DST-Nanomission programme of Department of Science and Technology, Government of India (DST/NM/TUE/QM-1/2019). KW and TT acknowledge support from the JSPS KAKENHI (Grant Numbers 21H05233 and 23H02052) and World Premier International Research Center Initiative (WPI), MEXT, Japan.

REFERENCES

(1) Cao, Y.; Fatemi, V.; Fang, S.; Watanabe, K.; Taniguchi, T.; Kaxiras, E.; Jarillo-Herrero, P. Unconventional Superconductivity in Magic-Angle Graphene Superlattices. *Nature* **2018**, *556*, 43−50.

(2) Cao, Y.; Fatemi, V.; Demir, A.; Fang, S.; Tomarken, S. L.; Luo, J. Y.; Sanchez-Yamagishi, J. D.; Watanabe, K.; Taniguchi, T.; Kaxiras, E.; Ashoori, R. C.; Jarillo-Herrero, P. Correlated Insulator Behaviour at Half-filling in Magic-Angle Graphene Superlattices. *Nature* **2018**, *556*, 80−84.

(3) Sharpe, A. L.; Fox, E. J.; Barnard, A. W.; Finney, J.; Watanabe, K.; Taniguchi, T.; Kastner, M. A.; Goldhaber-Gordon, D. Emergent Ferromagnetism Near Three-Quarters Filling in Twisted Bilayer Graphene. *Science* **2019**, *365*, 605−608.

(4) Serlin, M.; Tschirhart, C. L.; Polshyn, H.; Zhang, Y.; Zhu, J.; Watanabe, K.; Taniguchi, T.; Balents, L.; Young, A. F. Intrinsic Quantized Anomalous Hall Effect in a Moiré Heterostructure. *Science* **2020**, *367*, 900−903.

(5) Bistritzer, R.; MacDonald, A. H. Moiré Bands in Twisted Double-Layer Graphene. *Proc. Natl. Acad. Sci. U. S. A.* **2011**, *108*, 12233−12237.

(6) Yoo, H.; et al. Atomic and Electronic Reconstruction at the van der Waals Interface in Twisted Bilayer Graphene. *Nat. Mater.* **2019**, *18*, 448−453.

(7) Ahn, S. J.; Moon, P.; Kim, T.-H.; Kim, H.-W.; Shin, H.-C.; Kim, E. H.; Cha, H. W.; Kahng, S.-J.; Kim, P.; Koshino, M.; Son, Y.-W.; Yang, C.-W.; Ahn, J. R. Dirac Electrons in a Dodecagonal Graphene Quasicrystal. *Science* **2018**, *361*, 782−786.

(8) Yao, W.; Wang, E.; Bao, C.; Zhang, Y.; Zhang, K.; Bao, K.; Chan, C. K.; Chen, C.; Avila, J.; Asensio, M. C.; Zhu, J.; Zhou, S. Quasicrystalline 30° Twisted Bilayer Graphene as an Incommensurate Superlattice with Strong Interlayer Coupling. *Proc. Natl. Acad. Sci. U. S. A.* **2018**, *115*, 6928−6933.

(9) Pezzini, S.; Mišeikis, V.; Piccinini, G.; Forti, S.; Pace, S.; Engelke, R.; Rossella, F.; Watanabe, K.; Taniguchi, T.; Kim, P.; Coletti, C. 30°-Twisted Bilayer Graphene Quasicrystals from Chemical Vapor Deposition. *Nano Lett.* **2020**, *20*, 3313−3319.

(10) Utama, M. I. B.; et al. Visualization of the Flat Electronic Band in Twisted Bilayer Graphene Near the Magic-Angle Twist. *Nat. Phys.* **2021**, *17*, 184−188.

(11) Jiang, Y.; Lai, X.; Watanabe, K.; Taniguchi, T.; Haule, K.; Mao, J.; Andrei, E. Y. Charge Order and Broken Rotational Symmetry in Magic-Angle Twisted Bilayer Graphene. *Nature* **2019**, *573*, 91−95.

(12) Kerelsky, A.; McGilly, L. J.; Kennes, D. M.; Xian, L.; Yankowitz, M.; Chen, S.; Watanabe, K.; Taniguchi, T.; Hone, J.; Dean, C.; Rubio, A.; Pasupathy, A. N. Maximized Electron Interactions at the Magic Angle in Twisted Bilayer Graphene. *Nature* **2019**, *572*, 95−100.

(13) Choi, Y.; Kemmer, J.; Peng, Y.; Thomson, A.; Arora, H.; Polski, R.; Zhang, Y.; Ren, H.; Alicea, J.; Refael, G.; von Oppen, F.; Watanabe, K.; Taniguchi, T.; Nadj-Perge, S. Electronic Correlations in Twisted Bilayer Graphene Near the Magic Angle. *Nat. Phys.* **2019**, *15*, 1174−1180.

(14) Xie, Y.; Lian, B.; Jäck, B.; Liu, X.; Chiu, C.-L.; Watanabe, K.; Taniguchi, T.; Bernevig, B. A.; Yazdani, A. Spectroscopic Signatures of Many-Body Correlations in Magic-Angle Twisted Bilayer Graphene. *Nature* **2019**, *572*, 101−105.

(15) Wong, D.; Nuckolls, K. P.; Oh, M.; Lian, B.; Xie, Y.; Jeon, S.; Watanabe, K.; Taniguchi, T.; Bernevig, B. A.; Yazdani, A. Cascade of Electronic Transitions in Magic-Angle Twisted Bilayer Graphene. *Nature* **2020**, *582*, 198−202.

(16) Zondiner, U.; Rozen, A.; Rodan-Legrain, D.; Cao, Y.; Queiroz, R.; Taniguchi, T.; Watanabe, K.; Oreg, Y.; von Oppen, F.; Stern, A.; Berg, E.; Jarillo-Herrero, P.; Ilani, S. Cascade of Phase Transitions and Dirac Revivals in Magic-Angle Graphene. *Nature* **2020**, *582*, 203−208.

(17) Choi, Y.; Kim, H.; Peng, Y.; Thomson, A.; Lewandowski, C.; Polski, R.; Zhang, Y.; Arora, H. S.; Watanabe, K.; Taniguchi, T.; Alicea, J.; Nadj-Perge, S. Correlation-Driven Topological Phases in Magic-Angle Twisted Bilayer Graphene. *Nature* **2021**, *589*, 536−541.

(18) Nuckolls, K. P.; Oh, M.; Wong, D.; Lian, B.; Watanabe, K.; Taniguchi, T.; Bernevig, B. A.; Yazdani, A. Strongly Correlated Chern Insulators in Magic-Angle Twisted Bilayer Graphene. *Nature* **2020**, *588*, 610−615.

(19) Lisi, S.; et al. Observation of Flat Bands in Twisted Bilayer Graphene. *Nat. Phys.* **2021**, *17*, 189−193.

(20) Sato, K.; Hayashi, N.; Ito, T.; Masago, N.; Takamura, M.; Morimoto, M.; Maekawa, T.; Lee, D.; Qiao, K.; Kim, J.; Nakagahara, K.; Wakabayashi, K.; Hibino, H.; Norimatsu, W. Observation of a Flat Band and Bandgap in Millimeter-Scale Twisted Bilayer Graphene. *Communications Materials* **2021**, *2*, 117.

(21) Ferrari, A. C.; Meyer, J. C.; Scardaci, V.; Casiraghi, C.; Lazzeri, M.; Mauri, F.; Piscanec, S.; Jiang, D.; Novoselov, K. S.; Roth, S.; Geim, A. K. Raman Spectrum of Graphene and Graphene Layers. *Phys. Rev. Lett.* **2006**, *97*, 187401.

(22) Ferrari, A. C. Raman Spectroscopy of Graphene and Graphite: Disorder, Electron−Phonon Coupling, Doping and Nonadiabatic Effects. *Solid State Commun.* **2007**, *143*, 47−57.

(23) Eckmann, A.; Felten, A.; Mishchenko, A.; Britnell, L.; Krupke, R.; Novoselov, K. S.; Casiraghi, C. Probing the Nature of Defects in Graphene by Raman Spectroscopy. *Nano Lett.* **2012**, *12*, 3925−3930.

(24) Lui, C. H.; Li, Z.; Chen, Z.; Klimov, P. V.; Brus, L. E.; Heinz, T. F. Imaging Stacking Order in Few-Layer Graphene. *Nano Lett.* **2011**, *11*, 164−169.

(25) Poncharal, P.; Ayari, A.; Michel, T.; Sauvajol, J.-L. Raman Spectra of Misoriented Bilayer Graphene. *Phys. Rev. B* **2008**, *78*, 113407.

(26) Cong, C.; Yu, T.; Sato, K.; Shang, J.; Saito, R.; Dresselhaus, G. F.; Dresselhaus, M. S. Raman Characterization of ABA- and ABC-Stacked Trilayer Graphene. *ACS Nano* **2011**, *5*, 8760−8768.

(27) Podila, R.; Rao, R.; Tsuchikawa, R.; Ishigami, M.; Rao, A. M. Raman Spectroscopy of Folded and Scrolled Graphene. *ACS Nano* **2012**, *6*, 5784−5790.

(28) Gupta, A. K.; Tang, Y.; Crespi, V. H.; Eklund, P. C. Nondispersive Raman D Band Activated by Well-Ordered Interlayer Interactions in Rotationally Stacked Bilayer Graphene. *Phys. Rev. B* **2010**, *82*, 241406.

(29) Carozo, V.; Almeida, C. M.; Ferreira, E. H. M.; Cançado, L. G.; Achete, C. A.; Jorio, A. Raman Signature of Graphene Superlattices. *Nano Lett.* **2011**, *11*, 4527−4534.

(30) Ramnani, P.; Neupane, M. R.; Ge, S.; Balandin, A. A.; Lake, R. K.; Mulchandani, A. Raman Spectra of Twisted CVD Bilayer Graphene. *Carbon* **2017**, *123*, 302−306.

(31) Lu, C.-C.; Lin, Y.-C.; Liu, Z.; Yeh, C.-H.; Suenaga, K.; Chiu, P.-W. Twisting Bilayer Graphene Superlattices. *ACS Nano* **2013**, *7*, 2587−2594.

(32) Zhou, W.-G.; Leng, Y.-C.; Liu, L.-X.; Yang, M.-M.; Liu, W.; Liu, J.-L.; Zhao, P.; Liu, Y.; Wang, L.-L.; Shang, Y.-X.; Li, X.-L.; Zhao, X.-H.; Liu, X.-L.; Xu, Y. Twist Angle Dependent Absorption Feature Induced by Interlayer Rotations in CVD Bilayer Graphene. *Nanophotonics* **2021**, *10*, 2695−2703.

(33) He, R.; Chung, T.-F.; Delaney, C.; Keiser, C.; Jauregui, L. A.; Shand, P. M.; Chancey, C. C.; Wang, Y.; Bao, J.; Chen, Y. P. Observation of Low Energy Raman Modes in Twisted Bilayer Graphene. *Nano Lett.* **2013**, *13*, 3594−3601.

https://doi.org/10.1021/acsnano.3c08344
ACS Nano 2024, 18, 4756−4764

(34) Moutinho, M. V. O.; Venezuela, P.; Pimenta, M. A. Raman Spectroscopy of Twisted Bilayer Graphene. *C* **2021**, *7*, 10.
(35) Jorio, A.; Cançado, L. G. Raman Spectroscopy of Twisted Bilayer Graphene. *Solid State Commun.* **2013**, *175*−*176*, 3−12.
(36) Xu, B.; Hao, H.; Huang, J.; Zhao, Y.; Yang, T.; Zhang, J.; Tong, L. Twist-Induced New Phonon Scattering Pathways in Bilayer Graphene Probed by Helicity-Resolved Raman Spectroscopy. *J. Phys. Chem. C* **2022**, *126*, 10487−10493.
(37) Yeh, C.-H.; Lin, Y.-C.; Nayak, P. K.; Lu, C.-C.; Liu, Z.; Suenaga, K.; Chiu, P.-W. Probing Interlayer Coupling in Twisted Single-Crystal Bilayer Graphene by Raman Spectroscopy. *J. Raman Spectrosc.* **2014**, *45*, 912−917.
(38) Cong, C.; Yu, T. Evolution of Raman G and G' (2D) Modes in Folded Graphene Layers. *Phys. Rev. B* **2014**, *89*, 235430.
(39) Havener, R. W.; Zhuang, H.; Brown, L.; Hennig, R. G.; Park, J. Angle-Resolved Raman Imaging of Interlayer Rotations and Interactions in Twisted Bilayer Graphene. *Nano Lett.* **2012**, *12*, 3162−3167.
(40) Kim, K.; Coh, S.; Tan, L. Z.; Regan, W.; Yuk, J. M.; Chatterjee, E.; Crommie, M. F.; Cohen, M. L.; Louie, S. G.; Zettl, A. Raman Spectroscopy Study of Rotated Double-Layer Graphene: Misorientation-Angle Dependence of Electronic Structure. *Phys. Rev. Lett.* **2012**, *108*, 246103.
(41) Ni, Z.; Wang, Y.; Yu, T.; You, Y.; Shen, Z. Reduction of Fermi Velocity in Folded Graphene Observed by Resonance Raman Spectroscopy. *Phys. Rev. B* **2008**, *77*, 235403.
(42) Wang, Y.; et al. Resonance Raman Spectroscopy of G-Line and Folded Phonons in Twisted Bilayer Graphene with Large Rotation Angles. *Appl. Phys. Lett.* **2013**, *103*, 123101.
(43) Moutinho, M. V. O.; Eliel, G. S. N.; Righi, A.; Gontijo, R. N.; Paillet, M.; Michel, T.; Chiu, P.-W.; Venezuela, P.; Pimenta, M. A. Resonance Raman Enhancement by the Intralayer and Interlayer Electron−Phonon Processes in Twisted Bilayer Graphene. *Sci. Rep.* **2021**, *11*, 17206.
(44) Eliel, G. S. N.; Moutinho, M. V. O.; Gadelha, A. C.; Righi, A.; Campos, L. C.; Ribeiro, H. B.; Chiu, P.-W.; Watanabe, K.; Taniguchi, T.; Puech, P.; Paillet, M.; Michel, T.; Venezuela, P.; Pimenta, M. A. Intralayer and Interlayer Electron−Phonon Interactions in Twisted Graphene Heterostructures. *Nat. Commun.* **2018**, *9*, 1221.
(45) Campos-Delgado, J.; Cançado, L. G.; Achete, C. A.; Jorio, A.; Raskin, J.-P. Raman Scattering Study of the Phonon Dispersion in Twisted Bilayer Graphene. *Nano Research* **2013**, *6*, 269−274.
(46) Huang, S.; Yankowitz, M.; Chattrakun, K.; Sandhu, A.; LeRoy, B. J. Evolution of the Electronic Band Structure of Twisted Bilayer Graphene upon Doping. *Sci. Rep.* **2017**, *7*, 7611.
(47) SchäPers, A.; Sonntag, J.; Valerius, L.; Pestka, B.; Strasdas, J.; Watanabe, K.; Taniguchi, T.; Wirtz, L.; Morgenstern, M.; Beschoten, B.; Dolleman, R. J.; Stampfer, C. Raman Imaging of Twist Angle Variations in Twisted Bilayer Graphene at Intermediate Angles. *2D Materials* **2022**, *9*, 045009.
(48) Zhang, X.; Zhang, R.; Wang, Y.; Zhang, Y.; Jiang, T.; Deng, C.; Zhang, X.; Qin, S. In-Plane Anisotropy in Twisted Bilayer Graphene Probed by Raman Spectroscopy. *Nanotechnology* **2019**, *30*, 435702.
(49) Barbosa, T. C.; Gadelha, A. C.; Ohlberg, D. A. A.; Watanabe, K.; Taniguchi, T.; Medeiros-Ribeiro, G.; Jorio, A.; Campos, L. C. Raman Spectra of Twisted Bilayer Graphene Close to the Magic Angle. *2D Materials* **2022**, *9*, 025007.
(50) Pizzocchero, F.; Gammelgaard, L.; Jessen, B. S.; Caridad, J. M.; Wang, L.; Hone, J.; Bøggild, P.; Booth, T. J. The Hot Pick-Up Technique for Batch Assembly of van der Waals Heterostructures. *Nat. Commun.* **2016**, *7*, 11894.
(51) Hicks, J.; Sprinkle, M.; Shepperd, K.; Wang, F.; Tejeda, A.; Taleb-Ibrahimi, A.; Bertran, F.; Fèvre, P. L.; de Heer, W. A.; Berger, C.; Conrad, E. H. Symmetry Breaking in Commensurate Graphene Rotational Stacking: Comparison of Theory and Experiment. *Phys. Rev. B* **2011**, *83*, 205403.
(52) Uchida, K.; Furuya, S.; Iwata, J.-I.; Oshiyama, A. Atomic Corrugation and Electron Localization Due to Moiré Patterns in Twisted Bilayer Graphenes. *Phys. Rev. B* **2014**, *90*, 155451.
(53) Luican, A.; Li, G.; Reina, A.; Kong, J.; Nair, R. R.; Novoselov, K. S.; Geim, A. K.; Andrei, E. Y. Single-Layer Behavior and Its Breakdown in Twisted Graphene Layers. *Phys. Rev. Lett.* **2011**, *106*, 126802.
(54) Malard, L.; Pimenta, M.; Dresselhaus, G.; Dresselhaus, M. Raman Spectroscopy in Graphene. *Phys. Rep.* **2009**, *473*, 51−87.
(55) Kresse, G.; Furthmüller, J. Efficiency of Ab-Initio Total Energy Calculations for Metals And Semiconductors Using a Plane-Wave Basis Set. *Comput. Mater. Sci.* **1996**, *6*, 15−50.
(56) Kresse, G.; Furthmüller, J. Efficient Iterative Schemes for Ab Initio Total-Energy Calculations Using a Plane-Wave Basis Set. *Phys. Rev. B* **1996**, *54*, 11169−11186.
(57) Ould NE, M. L.; Boujnah, M.; Benyoussef, A.; Kenz, A. E. Electronic and Electrical Conductivity of AB and AA-Stacked Bilayer Graphene with Tunable Layer Separation. *Journal of Superconductivity and Novel Magnetism* **2017**, *30*, 1263−1267.
(58) Popov, V. N. Raman Bands of Twisted Bilayer Graphene. *J. Raman Spectrosc.* **2018**, *49*, 31−35.
(59) Brihuega, I.; Mallet, P.; González-Herrero, H.; Trambly de Laissardière, G.; Ugeda, M. M.; Magaud, L.; Gómez-Rodríguez, J. M.; Ynduráin, F.; Veuillen, J.-Y. Unraveling the Intrinsic and Robust Nature of van Hove Singularities in Twisted Bilayer Graphene by Scanning Tunneling Microscopy and Theoretical Analysis. *Phys. Rev. Lett.* **2012**, *109*, 196802.
(60) Popov, V. N. Two-Phonon Raman Bands of Bilayer Graphene: Revisited. *Carbon* **2015**, *91*, 436−444.
(61) Samsonidze, G. G.; Saito, R.; Jorio, A.; Filho, A. G. S.; Grüneis, A.; Pimenta, M. A.; Dresselhaus, G.; Dresselhaus, M. S. Phonon Trigonal Warping Effect in Graphite and Carbon Nanotubes. *Phys. Rev. Lett.* **2003**, *90*, 027403.
(62) Jorio, A.; Saito, R.; Hafner, J. H.; Lieber, C. M.; Hunter, M.; McClure, T.; Dresselhaus, G.; Dresselhaus, M. S. Determination of Isolated Single-Wall Carbon Nanotubes by Resonant Raman Scattering. *Phys. Rev. Lett.* **2001**, *86*, 1118−1121.
(63) Cong, C.; Yu, T.; Saito, R.; Dresselhaus, G. F.; Dresselhaus, M. S. Second-Order Overtone and Combination Raman Modes of Graphene Layers in the Range of 1690 - 2150 cm^{-1}. *ACS Nano* **2011**, *5*, 1600−1605.
(64) Rao, R.; Podila, R.; Tsuchikawa, R.; Katoch, J.; Tishler, D.; Rao, A. M.; Ishigami, M. Effects of Layer Stacking on the Combination Raman Modes in Graphene. *ACS Nano* **2011**, *5*, 1594−1599.
(65) Woods, C. R.; et al. Commensurate−Incommensurate Transition in Graphene on Hexagonal Boron Nitride. *Nat. Phys.* **2014**, *10*, 451−456.
(66) Kresse, G.; Joubert, D. From Ultrasoft Pseudopotentials to the Projector Augmented-Wave Method. *Phys. Rev. B* **1999**, *59*, 1758−1775.
(67) Blöchl, P. E. Projector Augmented-Wave Method. *Phys. Rev. B* **1994**, *50*, 17953−17979.
(68) Perdew, J. P.; Burke, K.; Ernzerhof, M. Generalized Gradient Approximation Made Simple. *Phys. Rev. Lett.* **1996**, *77*, 3865−3868.
(69) Grimme, S. Semiempirical GGA-Type Density Functional Constructed with a Long-Range Dispersion Correction. *J. Comput. Chem.* **2006**, *27*, 1787−1799.
(70) Monkhorst, H. J.; Pack, J. D. Special Points for Brillouin-Zone Integrations. *Phys. Rev. B* **1976**, *13*, 5188−5192.

https://doi.org/10.1021/acsnano.3c08344
ACS Nano 2024, 18, 4756−4764